CDISC Remote Design Method to Simulate Aircraft Interference Effects for the CATNLF Flight Test

Michelle N. Banchy[1], Richard L. Campbell[2], Brett R. Hiller[3], and Michael D. Bozeman[4]
NASA Langley Research Center, Hampton, Virginia, 23681

The Crossflow Attenuated Natural Laminar Flow (CATNLF) flight test is an experimental evaluation of a laminar flow design approach that will be conducted on a small transonic wing-like model suspended from the Centerline Instrumented Pylon (CLIP) underneath an F-15 vehicle. The upcoming flight test is anticipated to provide experimental data that may be useful for transition prediction code calibrations or laminar flow computational studies. For the computational results to be reliable, relevant aerodynamics must be included in the simulations. It has been shown that the F-15 vehicle produces a notable aerodynamic influence on the CATNLF test article, and that removing the F-15 vehicle from the simulation significantly alters the laminar flow behavior. Because the F-15 vehicle is not a publicly-releasable geometry, if the CATNLF flight test dataset is to be widely used by the community, an alternative method to ensure that the CATNLF test article flight configuration aerodynamics is properly modeled is required. The objective of this research is to use the CDISC aerodynamic design tool to perform a remote design of a surface that would replicate the aerodynamic influence on the CATNLF test article. This new design approach, referred to as the Equivalent Loading via Interference Surface Effects (ELISE), is presented in this paper, including the details on the design setup and results. The ELISE design successfully reproduced the F-15 influence on the CATNLF test article, with predicted transition location within an average of 4% chord of the full flight configuration. An off-design assessment is included for small perturbations in Mach and sideslip angle that suggest the ELISE design can cover a reasonable range of expected flight conditions with the same geometry. This paper is intended to explain the design approach, as well as show results that can be expected when utilizing the ELISE design method.

Nomenclature

Acronyms

BLSTA3D	=	Boundary Layer code for Stability Analysis 3D, boundary layer profile solver
CATNLF	=	Crossflow Attenuated Natural Laminar Flow
CDISC	=	Constrained Direct Iterative Surface Curvature, design module
CF	=	Crossflow
CLIP	=	Centerline Instrumented Pylon
CRM-NLF	=	Common Research Model with Natural Laminar Flow
ELISE	=	Equivalent Loading via Surface Interference Effects
LASTRAC	=	Langley Stability and Transition Analysis Code, transition prediction software
LFC	=	Laminar Flow Control
MAC	=	Mean Aerodynamic Chord
NASA	=	National Aeronautics and Space Administration
NLF	=	Natural Laminar Flow
RANS	=	Reynolds-averaged Navier-Stokes
ReHEAT	=	Resistive Heating for the Evaluation of Aerodynamic Transition
SWLF	=	Swept-Wing Laminar Flow

[1] Research Aerospace Engineer, NASA Langley Research Center, Configuration Aerodynamics Branch, AIAA Member.
[2] Senior Research Engineer, NASA Langley Research Center, Configuration Aerodynamics Branch, AIAA Associate Fellow.
[3] Research Aerospace Engineer, NASA Langley Research Center, Configuration Aerodynamics Branch, AIAA Member.
[4] Research Aerospace Engineer, NASA Langley Research Center, Configuration Aerodynamics Branch, AIAA Member.

SWT = Supersonic Wind Tunnel
TS = Tollmien-Schlichting
USM3D = Unstructured Mesh 3D, Navier-Stokes flow solver

Symbols

α = Angle of attack, degrees
β = Sideslip angle, degrees
c = Chord length, feet
C_P = Pressure coefficient
deg = Degree
Δ = Difference
η = Semispan location nondimensionalized by semispan length
h/c = Height of bump nondimensionalized by local chord
Re_{MAC} = Reynolds number based on mean aerodynamic chord
x/c = x-location nondimensionalized by local chord
$(x/c)_{Transition}$ = x-location of transition nondimensionalized by local chord

I. Introduction

LAMINAR flow technology has been the subject of several recent studies across the aerospace industry because of its potential to significantly improve vehicle performance. Laminar flow is known to reduce both the skin friction and profile drag of a component, and can be achieved through either natural laminar flow (NLF) or laminar flow control (LFC) methods. NLF is particularly advantageous as it often eliminates some negative multidisciplinary penalties associated with popular LFC options, such as suction systems that can add weight or mechanical complexity to the vehicle. NLF is being investigated in computational studies of next-generation aircraft to help meet emission reduction goals, as well as experimental wind tunnel and flight tests to validate performance goals and mature the technology. One significant challenge with maintaining large extents of NLF on some aircraft components is the presence of crossflow instabilities. Crossflow instabilities grow with sweep and Reynolds number, and are therefore a common occurrence on the main wing of a traditional transonic transport. For a vehicle to achieve the performance improvement potential available from NLF, these crossflow instabilities must be reduced or controlled to prolong the extents of laminar flow on the wing beyond the leading edge. The Crossflow Attenuated Natural Laminar Flow (CATNLF) Flight Test campaign is an ongoing effort led by NASA with the goal of advancing one method for obtaining NLF on transport wings, referred to as the CATNLF design method [1].

The CATNLF design method enables laminar flow by reducing the crossflow boundary layer instabilities at the leading edge of a wing, then prolongs the extent of laminar flow by controlling the Tollmein-Schlicting (TS) instabilities in the midchord region. The method relies on tailoring the wing geometry to produce specific pressure distributions that introduce a rapid flow acceleration at the leading edge to suppress crossflow growth. Prior to the flight test effort, the CATNLF method was developed in computational studies [2–3] and experimentally investigated in a high Reynolds number wind tunnel facility [4–7]. Using the CATNLF method, transonic transport configurations were designed that provided approximately 50% of laminar flow on the wing upper surface and offered on the order of 7–9% drag reduction. The data from the CATNLF wind tunnel test, commonly referred to as the Common Research Model with Natural Laminar Flow (CRM-NLF) wind tunnel test, have been publicly released and studied by the computational community [8]. Analysis of the CRM-NLF experimental data has provided initial confirmation of the computational predictions and the overall validity of the CATNLF approach to obtaining large extents of laminar flow on the main wing of a transonic transport vehicle.

Positive results from the wind tunnel test have led to the CATNLF Flight Test campaign, in which the team hopes to further advance the CATNLF technology by studying the concept in a flight environment. The test campaign is a series of three separate flight tests, each with unique hardware to accomplish a specific goal. All three flight tests are to be conducted at the NASA Armstrong Flight Research Center utilizing the F-15 Centerline Instrumented Pylon (CLIP) flight testbed, shown in Figure 1 [9]. The first two flights are risk reduction and support flights, and the third flight is the primary experiment. The first flight test, referred to as Resistive Heating for the Evaluation of Aerodynamic Transition (ReHEAT), used an existing test article that was painted with a heating layer to improve the laminar flow visualization in flight [10]. The ReHEAT flight test was successfully flown in 2019 and 2020, and confirmed the practicality and usefulness of the heating layer in the third flight test. The second flight test is the Flow Rake flight test, in which the team manufactured and instrumented a crucible-form test article to characterize the flow underneath the F-15 aircraft. The Flow Rake flight test is scheduled to fly in early 2024 and will provide valuable information (e.g., turbulence intensity, local Mach number, flow angle) necessary to understand the influence of the

F-15 on the test article. The third flight test is the primary experiment, and is referred to as the CATNLF Flight Test. The test article was designed using the CATNLF method at conditions representative of a transonic transport wing and is predicted to support large extents of laminar flow in flight [1]. For flight testing, the test article is instrumented with a variety of sensors to provide valuable data to better understand the technology and laminar flow physics. First flight for the CATNLF test article is presently anticipated in 2024. This third flight is the focus of this work. Figure 2 shows all three test articles from the CATNLF flight test campaign.

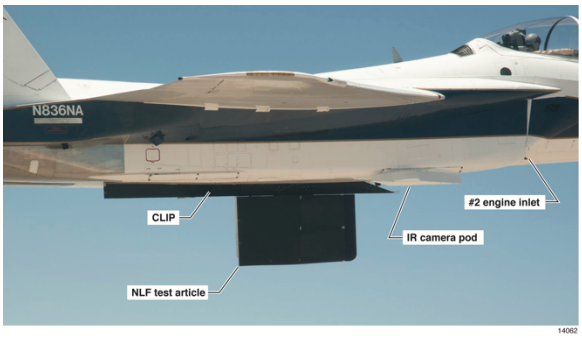

Figure 1. Photo of flight testbed showing the F-15 with undermounted CLIP and sample test article [Source: NASA, Ref. [9]].

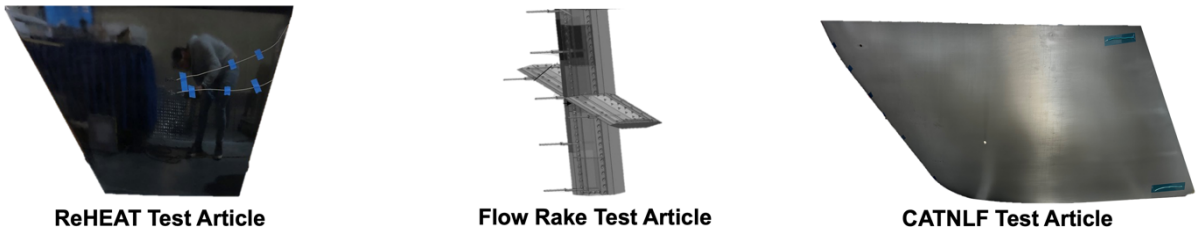

Figure 2. Images of the three unique test articles used in the CATNLF flight test campaign.

In addition to the technology development goals for the CATNLF flight test article, there is hope that the dataset can be used to further advance computational tools, specifically those used in transition prediction. One avenue toward this goal would be to publicly release the flight test data for the computational community to use in code evaluation or calibration, similar to the CRM-NLF dataset. Another route being pursued is to test the CATNLF flight test article in a wind tunnel after the flight testing is complete. This wind tunnel test would provide a dataset that would help isolate the impact of the environment on the laminar flow extents, and may be useful for understanding how to best model different environments in computational studies. Both of these approaches for advancing computational tool development would require the geometry of the test article to be provided, so that users of the dataset can model the configuration directly in their specific tool. The CATNLF test article was designed in the presence of the F-15 aircraft to ensure that impact of the flight testbed was accounted for in the design. The details of the test article design approach were previously published by Lynde (Banchy) et. al [1]. At present, the F-15 geometry is a controlled configuration that cannot be released publicly. However, without the presence of the F-15, the CATNLF test article does not maintain the same flow characteristics and transition behavior is significantly altered. This poses a significant challenge to the plan of providing a usable dataset to the community from the flight test data.

The work discussed in this paper is focused on exploring an alternative method for including the F-15 influence on the CATNLF test article. This work investigates a new remote design approach, referred to as Equivalent Loading via Interference Surface Effects (ELISE), which creates an arbitrary surface designed to reproduce the aerodynamic influence of the F-15 vehicle on the test article in flight. This paper will include an explanation of the ELISE design approach and a sample designed geometry. The sample designed geometry does not necessarily correspond to any future publicly-released geometry, but rather serves as an example of the new remote design strategy. Any publicly-released geometry would be anchored on the flight test data, which was not available at the time of this publication. Data will be presented that illustrate the effectiveness of the design at the design point and at near-cruise, off-design conditions. Discussions are also provided regarding the feasibility of using the ELISE design method for a wind tunnel test.

II. Design Approach

Designing an arbitrary surface to reproduce the aerodynamic interference of a complex vehicle like the F-15 involves several computational tools and a new strategy for remote design. This subsection will present the computational tools employed in this work, further discussion of the challenges this work aims to address, and the steps taken to complete the remote design.

A. Computational Tools

The computational toolset utilized in this work includes a flow solver, an aerodynamic design module, and transition prediction software that are coupled together to perform the design work, as illustrated in the flow chart in Figure 3. The flow solver selected for this work, USM3D-ME, is an unstructured, cell-centered, Reynolds-averaged Navier-Stokes (RANS) solver developed at the NASA Langley Research Center [11–12]. All flow solutions were obtained using mixed-element grids, which are described in the following *Problem Definition* subsection. The turbulence model utilized was the one-equation Spalart-Allmaras model with negative provisions, Rotation/Curvature (RC) correction, and the Quadratic Constitutive Relation (QCR-2000). For solutions that include the F-15 aircraft, the engines were simulated with powered-engine inflow/outflow boundary conditions.

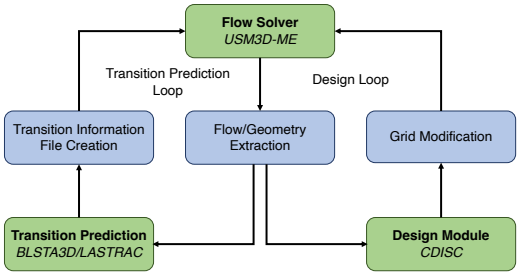

Figure 3. Flow chart of computational tools.

The aerodynamic design module for this work is referred to as CDISC, which is a knowledge-based design tool developed at the NASA Langley Research Center [13–14]. The design module is coupled with the flow solver and is an iterative process in which it will establish target pressure distributions, calculate the required geometry changes, morph the grid, and resubmit the altered grid for additional flow iterations. CDISC works off user-specified flow constraints, which create the target pressure distributions at specified design stations, and will apply user-specified geometry constraints to avoid unwanted geometry changes or features. CDISC uses prescribed sensitivity derivatives to determine the geometry changes required on the design surface based on the difference between the target and analysis pressures. The CDISC design tool has been used in a wide variety of design applications since its initial creation in the 1980s, including computational studies, wind tunnel model designs, and flight vehicle designs. While the tool has been used in a range of design applications, the most common design problem is direct design, in which CDISC is set up to directly alter the primary surface of interest. An example of a common direct design project that CDISC would be used for is a wing design case, where the design stations, target pressures, and geometric changes are made directly on the wing surface. The unique application of CDISC in this paper is referred to as remote design, in which the primary surface of interest is fixed, and the design is accomplished by altering a separate surface in order to provide aerodynamic influence on the primary surface. Additional information about the unique application and design approach are provided in the following subsection, *Remote Design Strategy*.

As discussed previously, the work presented in this paper is related to laminar flow research, which necessitates the use of laminar flow prediction software. For this work, a boundary layer solver, BLSTA3D, is coupled with the stability analysis and transition prediction code, LASTRAC. The boundary layer solver will calculate the laminar boundary layer velocity and temperature profiles based on surface pressure and geometry [15]. For the results in this paper, the boundary layer profiles were calculated using conical corrections to account for sweep and taper of the test article, and were based on pressures and geometry in the chordwise direction. LASTRAC calculates the instability growth associated with these boundary layer profiles [16]. For this work, two-dimensional Tollmien-Schlicting (TS) and stationary crossflow (CF) instability growth is considered using Linear Stability Theory, e^N method, accounting for compressibility effects but not curvature influence. Transition is assumed to occur when either TS or CF reach a user-selected critical N-factor. For this work, a critical N-factor of 10 was used to represent a flight environment. This approach to transition prediction is consistent with previous work, including the CRM-NLF wind tunnel test analysis, as well as the design of the CATNLF Flight Test article.

B. Problem Definition

The CATNLF test article was designed using a grid that included the F-15 vehicle with the idea that modeling the entire flight setup would offer the best chances of achieving the flight test objectives, namely observing large extents of laminar flow on the test article. This approach ensured that the test article accommodated any aerodynamic influence from the test setup, such as local Mach or flow angularity created by the F-15 at the CLIP location where the test article is mounted. Due to these interference effects, when the CATNLF test article is analyzed without the F-15 present, the aerodynamic and transition characteristics of the test article are significantly altered. As previously mentioned, there are anticipated uses of the flight test dataset in which access to the geometry would be required by a wide audience, such as publicly releasing the data for use in transition prediction code development. Unfortunately, it is not permissible that the F-15 geometry be provided openly, which is what necessitates the remote design capability developed in this paper.

To evaluate the aerodynamic influence the F-15 has on the CATNLF test article, two computational grids were developed. The first is referred to as the Flight Configuration, shown in Figure 4, and includes the full F-15 vehicle (gray), the CLIP (orange), and the mounted test article (blue). A grid refinement study was performed to ensure the test article was properly resolved and the mixed-element grid selected for use in this work has approximately 173 million cells. The second grid is referred to as the Isolated Configuration, which removes the F-15 vehicle so that only the CLIP (orange) and test article (blue) are modeled, and can be seen in Figure 5. In place of the F-15 vehicle, an inviscid plane is added (gray) where the juncture between the CLIP and F-15 would exist. This mixed-element Isolated Configuration grid is much smaller and less complex, with approximately 34 million cells. An attempt to isolate the influence of the F-15 was made by maintaining grid generation techniques between the Flight Configuration and the Isolated Configuration, and several relevant parameters were kept constant during grid generation to ensure similar resolution on the test article, such as average cell size, maximum cell stretch ratio, and maximum surface-curvature deviation. The solutions found in this report are all from the grids developed specifically for this work. It was observed that the new Flight Configuration grid produces slightly different aerodynamic predictions on the test article compared to the solutions used in the previously-published paper, which covered the test article design work [1]. These changes are not expected to significantly impact the flight test or computational study presented here, and is only mentioned to address any inconsistencies between predicted laminar flow extents on the test article between the previous report and the present work. It should also be noted that because the CATNLF test article is mounted vertically underneath the F-15, changes in F-15 angle of attack create an effective sweep change on the test article and changes in F-15 sideslip angle create an effective angle-of-attack change on the test article. The CATNLF test article is mounted to the CLIP at an F-15 sideslip angle of -8.2 deg (i.e., a test article angle of attack of +8.2 deg) so that the pilot can fly the F-15 straight and level during flight testing and still produce the desired load on the test article. Therefore, the primary design condition set in the flow solver is an angle of attack and sideslip of 0 degrees. This mounting angle is maintained between both the Full Configuration and Isolated Configuration grids.

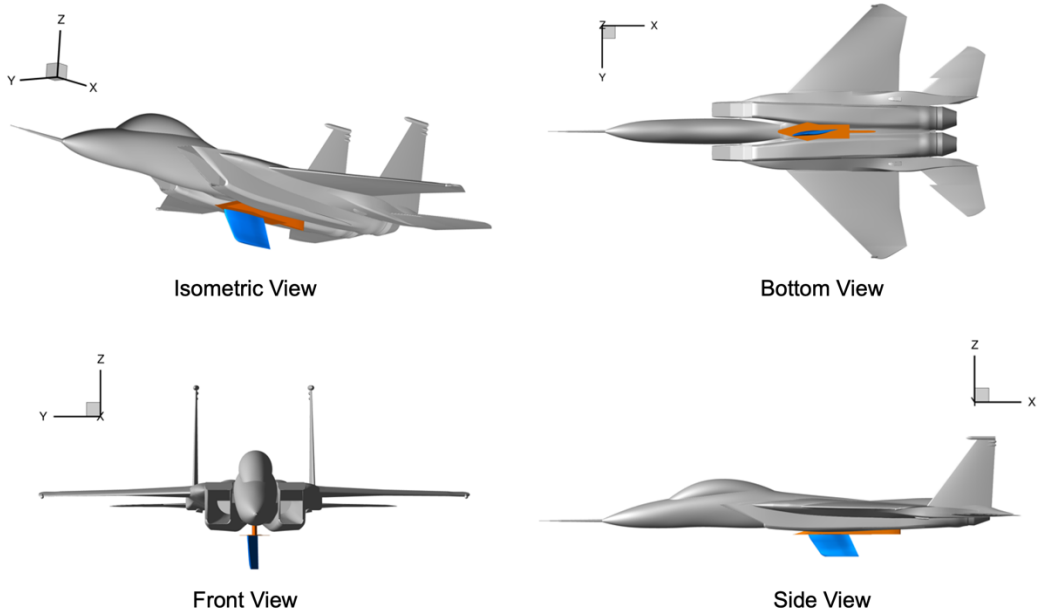

Figure 4. Views showing components included in the Flight Configuration grid, including the F-15 (gray), CLIP (orange), and CATNLF test article (blue).

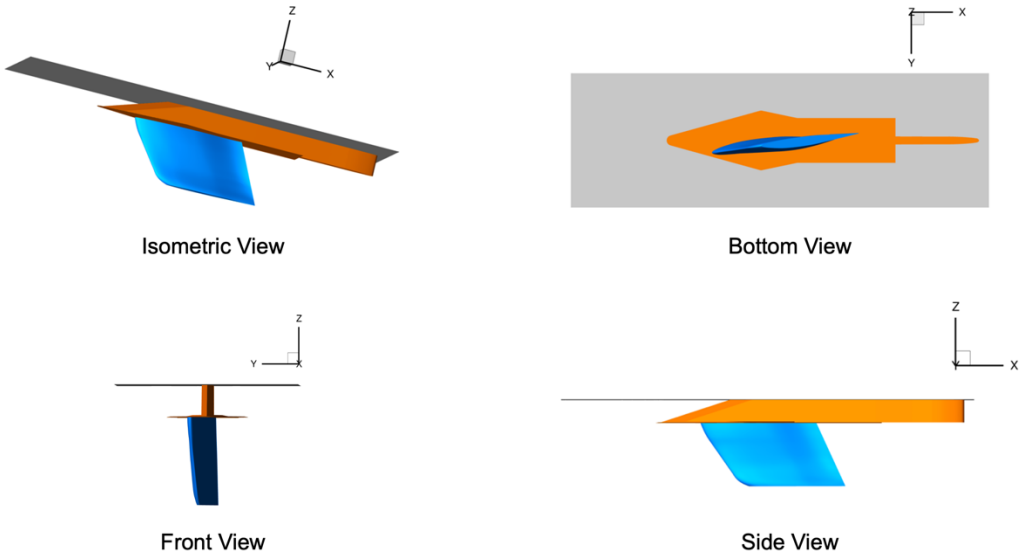

Figure 5. Views showing components included in the Isolated Configuration grid, including an inviscid flat plate (gray), CLIP (orange), and CATNLF test article (blue).

The two computational grids enable a direct comparison of the test article behavior with and without the F-15. For this work, 17 chordwise stations evenly spaced across the span of the test article were used for comparing various solutions and boundary layer instability calculations. In this paper, three spanwise stations on the test article will be used as examples, the location of which are shown in Figure 6. These three stations were selected because they are the locations of the static pressure ports on the test article, and therefore the locations where experimental pressure data will be acquired. Figure 7 shows the three sample surface pressures on the test article comparing the Flight Configuration (blue) and the Isolated Configuration (red). The pressure distributions clearly show the effect of not including the F-15 in the simulation, with the Isolated Configuration showing significant changes including a collapsed rooftop pressure leading to a farther forward shock, as well as a notable changes in pressure level suggesting a possible Mach shift between the solutions. Figure 8 shows the resulting differences in laminar flow characteristics via the N-factor growth of TS and CF. The test article was designed to gradually grow TS instabilities from the leading edge to the desired transition point, a behavior that can be seen in the Flight Configuration TS N-factor data. Without the F-15, the test article has adverse pressure gradients that cause the TS to grow much more rapidly than originally designed, significantly reducing the amount of laminar flow. The CF behavior is comparatively much less impacted by the absence of the F-15. The leading-edge CF growth is similar between the solutions, although consistently slightly higher on the Isolated Configuration. The largest difference in character for CF is seen after the initial growth and damping at the leading edge, where the Isolated Configuration enters a midchord regrowth region due to the change in pressure gradients without the F-15. While this midcord CF regrowth is not expected to be critical, it is not ideal to have such large changes in characteristics or trends between the solutions if the data are to be used for code calibrations. Figure 9 shows the predicted transition fronts with and without the F-15. The Flight Configuration is predicted to support laminar flow over 40.8% of the surface area, whereas the Isolated configuration only has 11.6% laminar flow. These results demonstrate that providing only the geometry in the Isolated Configuration would not be an adequate representation of the CATNLF test article in flight, and therefore, could not be used for correlation with the flight test dataset for laminar flow computational studies. It is preferred to maintain the shape of the test article to eliminate geometric changes from becoming a factor in any comparisons to the flight test data, so redesigning the shape of the test article in the Isolated Configuration grid is not a feasible option. This fact led to the present work, in which the aim is to create a surface that would match the F-15 aerodynamic interference on the fixed-geometry test article.

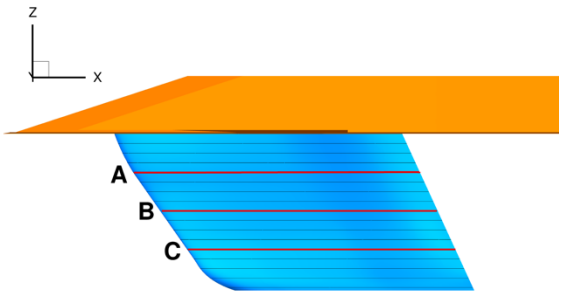

Figure 6. Station layout on the CATNLF test article, highlighting in red the 3 stations used as examples throughout this paper.

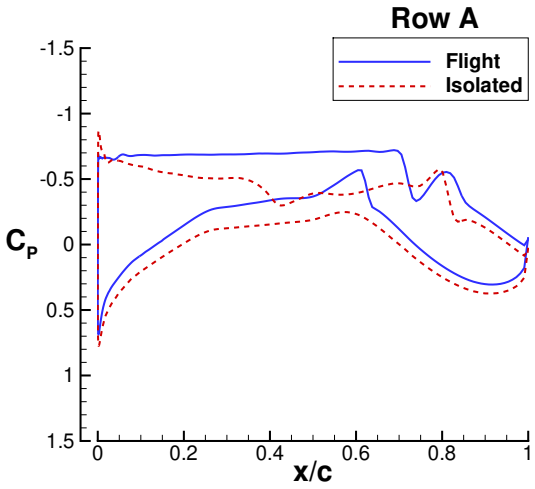

a. Row A pressure distributions.

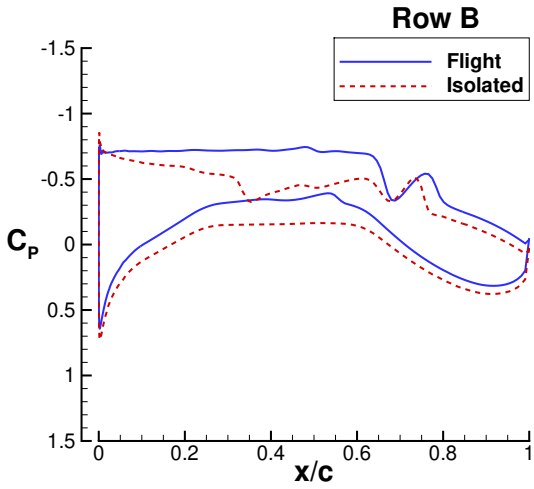

b. Row B pressure distributions.

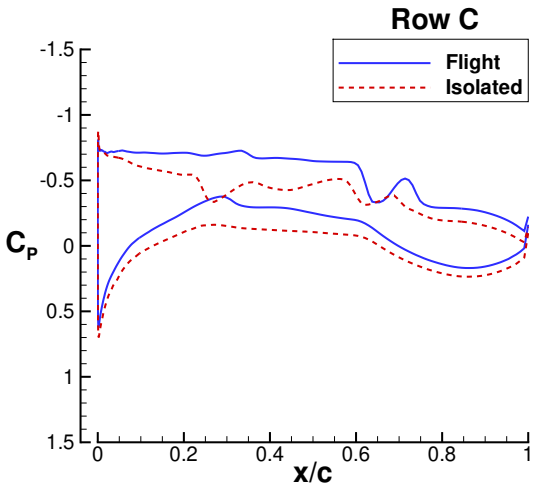

c. Row C pressure distributions.

Figure 7. Pressure distributions at the three example rows on the CATNLF test article, comparing the flow solution from the Flight Configuration grid (blue) and the Isolated Configuration grid (red).

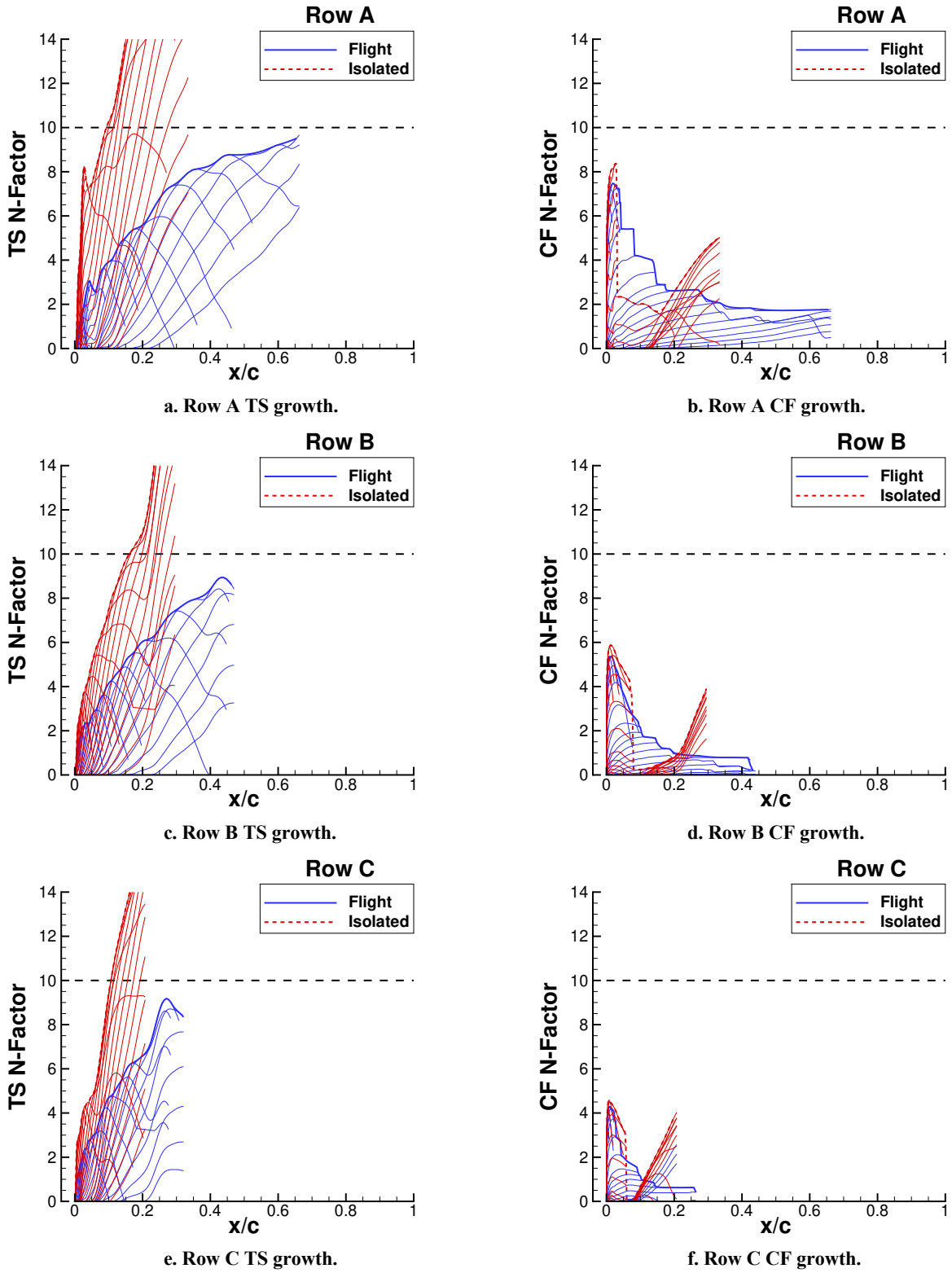

a. Row A TS growth.

b. Row A CF growth.

c. Row B TS growth.

d. Row B CF growth.

e. Row C TS growth.

f. Row C CF growth.

Figure 8. N-factor growth of both Tollmien-Schlicting (left) and crossflow (right) from the Flight Configuration grid (blue) and the Isolated Configuration grid (red). The horizontal dashed line at an N-factor of 10 represents the critical N-factor used in this work.

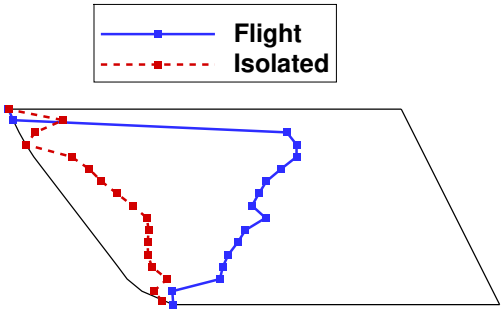

Figure 9. Planform view of the test article showing the predicted transition locations from the Flight Configuration grid (blue) and the Isolated Configuration grid (red).

C. Remote Design Strategy

A new remote design procedure was developed to accomplish the research objective of matching the CATNLF test article loading and flow characteristics by creating a surface that provides the same aerodynamic interference as the F-15. As mentioned, this new remote design process within CDISC is referred to as Equivalent Loading via Interference Surface Effects (ELISE).

The first task in setting up the design case was to determine the size of the ELISE surface, which is the area that CDISC will be allowed to alter during the design process. The ELISE surface size requirements are fairly unconstrained for use with a computational study. For the results presented in this paper, the ELISE surface size definition was based off the idea of using a similar surface in a wind tunnel environment, so the length and width of the surface is representative of the test sections in two possible facilities. The ELISE surface dimensions can be found in Table 1, along with some dimensions of the CLIP and test article for comparison. It should be noted that the results in this paper are only demonstrative of a surface that could be used in a computational study, and would not be suitable for a wind tunnel test. Discussions on alterations to the ELISE surface from this paper that would be required for a wind tunnel test are provided in the section, *Additional Considerations for Wind Tunnel Applications*.

Table 1. Dimensions of ELISE remote design setup.

ELISE Surface Length	21.4 ft
ELISE Surface Width	7.0 ft
CLIP Length	16.3 ft
CLIP Width	3.1 ft
CATNLF Test Article MAC	5.9 ft
CATNLF Test Article Span	3.3 ft

As discussed in the *Computational Tools* subsection, CDISC alters the geometry at the design stations to minimize the difference between the target pressures from CDISC and current analysis pressures from the flow solver. For this remote design work, the CDISC target pressures and geometry manipulation will be done only on the ELISE surface. Once the ELISE surface size was established, ten chordwise (streamwise direction) design stations were distributed across the width of the surface. The ELISE surface planform with the ten design stations can be seen in Figure 10.

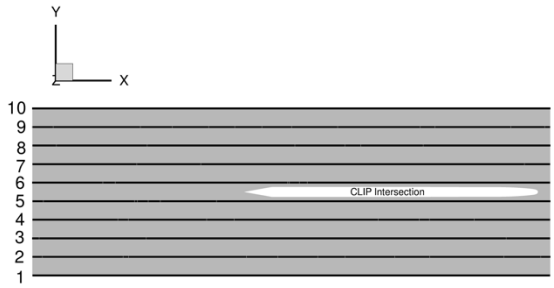

Figure 10. Planform view of the ELISE design surface setup showing the 10 stations used for the CDISC design process.

For use with CDISC, target pressure distributions are needed at each of the design stations to drive the geometry changes. The goal of the design is to mimic the F-15 interference with the ELISE surface, so the target pressures for ELISE were extracted from the F-15 flow solution. A flow solution on the Flight Configuration grid was obtained at the design condition of Mach 0.85, an angle-of-attack (α) and sideslip angle (β) of 0 degrees, and an altitude of 5,000 feet which results in a Reynolds number based on the CATNLF test article mean aerodynamic chord (Re_{MAC}) of 31 million. Surface pressures were extracted from the underside of the F-15 at the X-Y locations corresponding to the design stations on the ELISE surface, illustrated in Figure 11. These F-15 surface pressures were the starting point for the target pressures used within the design process with the hope that CDISC could alter the ELISE surface from a flat plane to a surface that creates the F-15 pressure field. Alterations were made to these target pressures as the design developed, described in the following *Design Results* section, in order to improve the correlation of the CATNLF test article between the two grids.

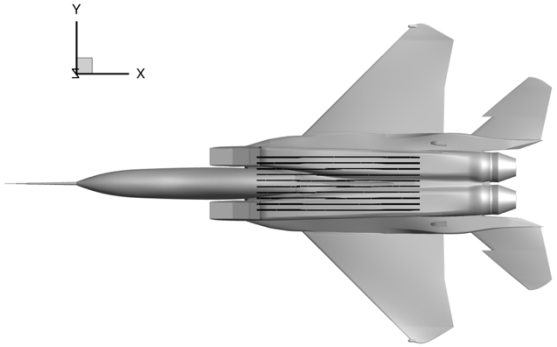

Figure 11. Bottom view of the F-15 vehicle showing the locations (black lines) that surface pressures were extracted to be used as target pressures with CDISC.

III. Design Results

The results presented in this paper are intended to serve as an example of the newly developed ELISE remote design process within CDISC. This subsection includes a discussion of the design, with emphasis on the impact to the CATNLF test article. Results from both the design point and off-design are included. The final geometry and analyses included in this paper, while representative of the capabilities and limitations, would not be the final geometry publicly released to the community. A new ELISE design would be performed once the flight test is concluded to ensure that the ELISE surface reproduces the CATNLF test article aerodynamic characteristics according to the experimental data.

A. Design Point

The design point for the ELISE surface was set to the same flow conditions as the primary design point for the CATNLF test article, which is Mach = 0.85, $\alpha = \beta = 0$ deg, altitude = 5,000 ft, and Re_{MAC} = 31 million. The Isolated Configuration grid was used for the design, with the previously described design station locations on the inviscid surface at the base of the CLIP. Once the design process began, it was discovered that several changes to the design region would be required to improve the robustness of the grid movement. The region outside the design space was fixed, which led to constraints to hold the geometry constant at the intersection edges. This included fixing the leading and trailing edges of all the design stations, as well as at the left-most and right-most stations (Stations 1 and 10). In addition to keeping the four edges of the ELISE surface flush with the original flat plane, it was observed that grid movement became a challenge for the tools when the design stations closest to the CLIP intersection (Stations 5 and 6) grew too large, so those two middle stations were also held flush with the original flat plate. There was a desire to minimize the size of the ELISE surface, mostly motivated by gathering knowledge for a future application of the design method for wind tunnel surfaces, which is discussed further in the following *Additional Considerations for Wind Tunnel Applications* section. This minimization effort led to further restrictions in the design region, including limiting the length to design only between 20% and 80% chord and limiting the width to designing only at the two stations on either side of the CLIP farther from the middle (Stations 2, 3, 8, and 9). Figure 12 illustrates the reduced design region for the ELISE surface geometry that CDISC was allowed to alter.

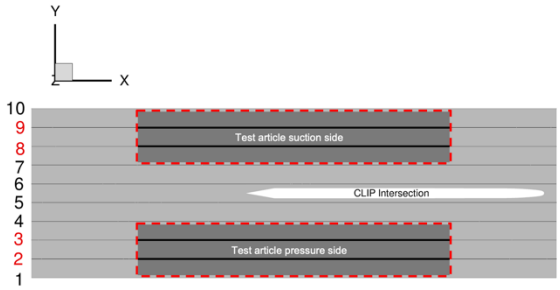

Figure 12. Planform view of the ELISE surface with the reduced design zone highlighted (dark gray with red boarder).

In addition to alterations to the design region, adjustments were made to the target pressures used by CDISC to guide the shape changes. As mentioned in the previous section, the original target pressures were extracted from the F-15 surface at the same X-Y locations as the ELISE surface design stations. Initial results from early designs showed what appeared to be a Mach shift on the CATNLF test article, suggesting that the designed ELISE surface was not adequately capturing the flow acceleration introduced by the F-15. In order to better capture this change in Mach from the F-15, the target pressures for the ELISE surface were altered to promote additional flow acceleration on the surface. The best results came from reducing the pressure (i.e., increasing Mach) of the target pressures with a chordwise variation. The chordwise variation used was a larger decrease in pressure toward the leading edge that was gradually reduced to no decrease at the trailing edge. These changes in target pressures are reflected in the results presented in this paper.

One hundred design cycles were used to allow CDISC to converge on a geometry that adequately produced the target pressure distributions. Figure 13 shows the pressure distributions at the four stations used for design, including the starting pressures (red) from the flat surface, the final design analysis pressures (black), and the target pressures (black symbols). One metric of a successful design in CDISC is the qualitative agreement between the design pressures and target pressures, which implies that CDISC was able to alter the geometry appropriately to change the solution from the original flat plate pressures to the desired target pressures. In general, reasonable agreement was achieved between the target pressures and final design pressures. Stations 8 and 9 are located on the side with the suction surface of the test article, which explains the higher velocities at those stations relative to Stations 2 and 3. The resulting geometry changes made by CDISC can also be seen in Figure 13. The geometry changes were more significant closer to the test article (Stations 3 and 8), where the target pressures required more acceleration. A three-dimensional view of the geometry changes in Figure 14 provides a visualization of the proportions of the final ELISE surface relative to the CLIP and CATNLF test article. Through the design process, two asymmetric bumps were added to the ELISE surface on either side of the test article, with the bump on the suction side of the test article being slightly lower than the bump on the test article pressure side. Table 2 reports the dimensions of the designed ELISE surface.

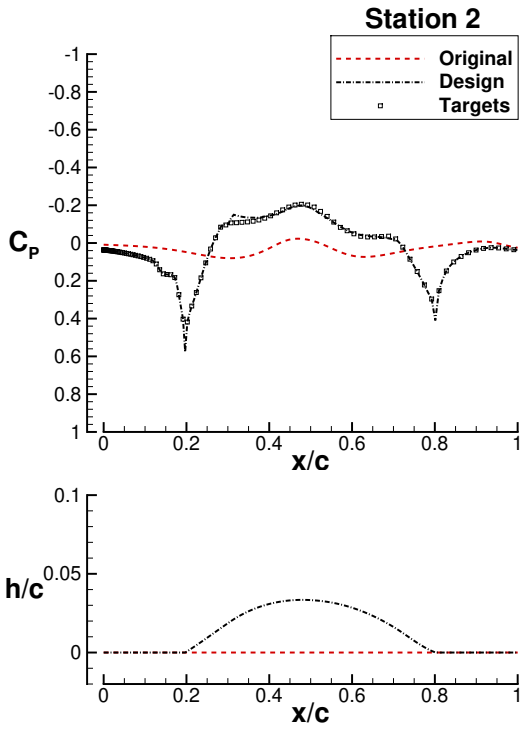

a. Station 2 pressures (top) and geometry (bottom).

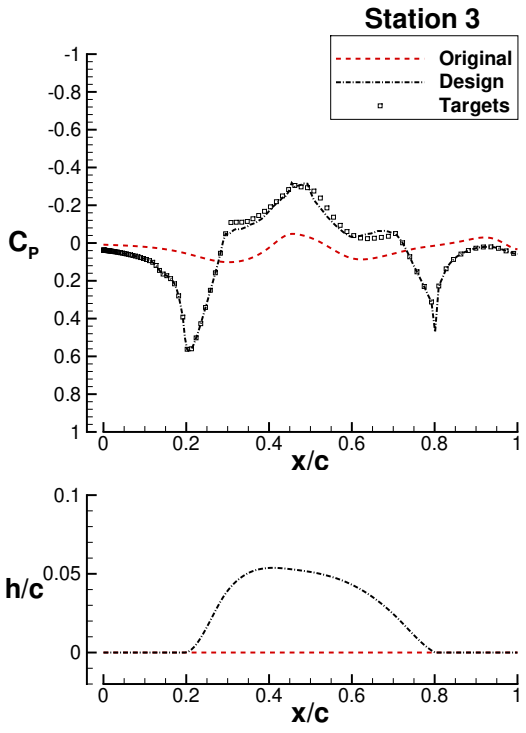

b. Station 3 pressures (top) and geometry (bottom).

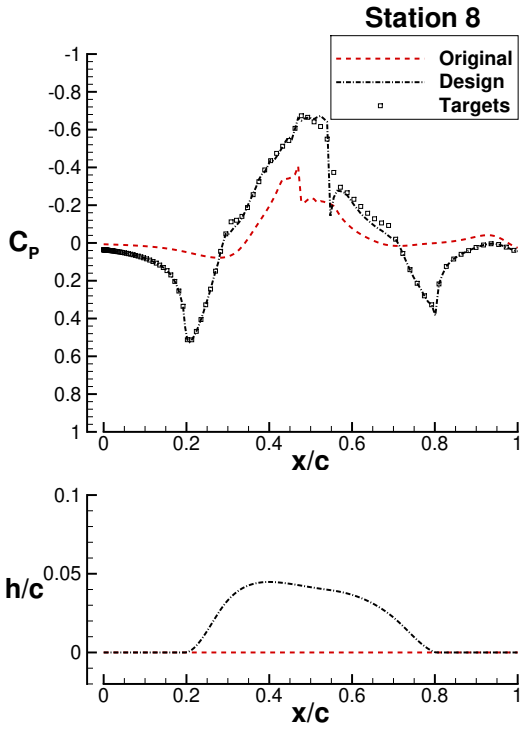

c. Station 8 pressures (top) and geometry (bottom).

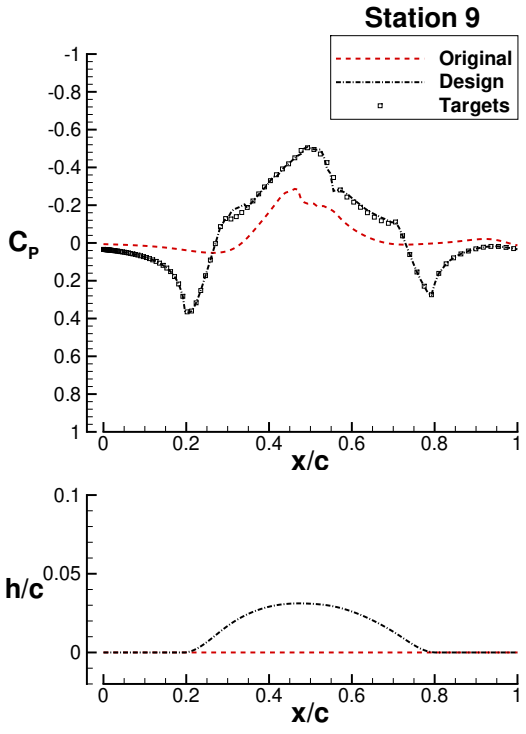

d. Station 9 pressures (top) and geometry (bottom).

Figure 13. Pressure distributions and geometry from the four stations used in design on the ELISE surface. The original solutions (red), which corresponds to the flat plate starting point, is shown with the final ELISE design shape (black). On the pressure distributions, the target pressures (black squares) used in the CDISC design process are included.

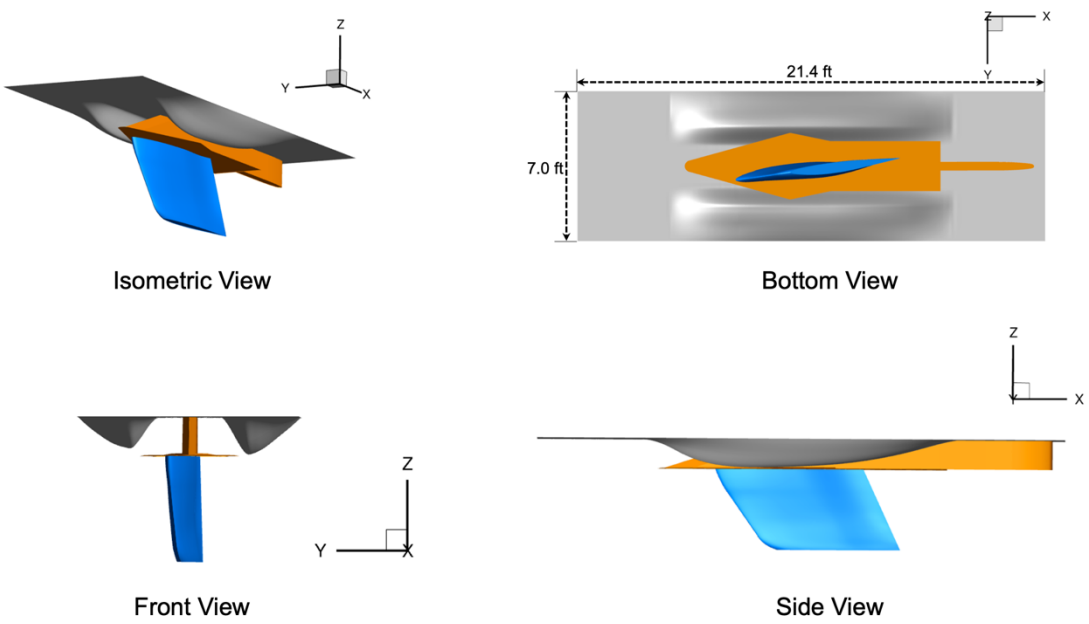

Figure 14. Views of the designed ELISE surface (gray) with the CLIP (orange) and test article (blue).

Table 2. Dimensions of the designed ELISE surface.

Designed Length	13.1 ft
Designed Width (Each Side)	1.7 ft
Designed Width (Total)	7.0 ft
Maximum Height (Test Article Suction Side)	2.0 ft
Maximum Height (Test Article Pressure Side)	2.4 ft

The primary metric of success for this remote design effort is based on the aerodynamic characteristics of the CATNLF test article. The three example pressure distributions along the span of the test article can be found in Figure 15, comparing the Flight Configuration (blue), the Isolated Configuration without the designed ELISE surface (red), and the Isolated Configuration with the ELISE design (black) solutions. No shape changes were made to the CATNLF test article, and the flow solver input conditions were identical between the solutions, implying that any changes in the CATNLF test article aerodynamics between the Isolated Configuration (red) and ELISE Design (black) results are purely resulting from aerodynamic influence from the nearby surfaces. It can be seen in the pressure distributions that the ELISE surface successfully alters the Isolated Configuration pressures to resemble the Flight Configuration. The primary surface of concern for this work was the suction side because that is the surface being studied for laminar flow, however, both pressure and suction side surfaces agree similarly well. It can be observed that a slight pressure level shift still exists between the Flight Configuration and ELISE Design solutions, indicating that there is likely still a slight Mach shift, with the F-15 vehicle imparting a slightly higher Mach influence than the ELISE surface. The more forward location of the shock in the ELISE Design solution supports the hypothesis of a slightly lower effective Mach as well. An additional difference can be seen at Row B and C where a slight pressure wiggle occurs on the suction surface ahead of the shock. The pressure wiggle can be seen on both the Flight Configuration and ELISE Design solutions, but the magnitude and chordwise location is slightly altered. The feature being shifted slightly downstream for the Flight Configuration solution again supports the Mach shift explanation, as previous results have shown that the pressure wiggle emanates from the wingtip and moves further aft as the freestream Mach is increased. While these features can be observed and explained, the overall agreement between the Flight Configuration and ELISE Design solutions clearly demonstrate the success of the ELISE remote design approach to replicate the F-15 aerodynamic interference. The minor differences that remain between the pressures are well beyond the magnitude of what is expected to be measurable and/or repeatable in the flight experiment pressure data, and are therefore believed to be acceptable differences for the intended use cases of the ELISE Design surface.

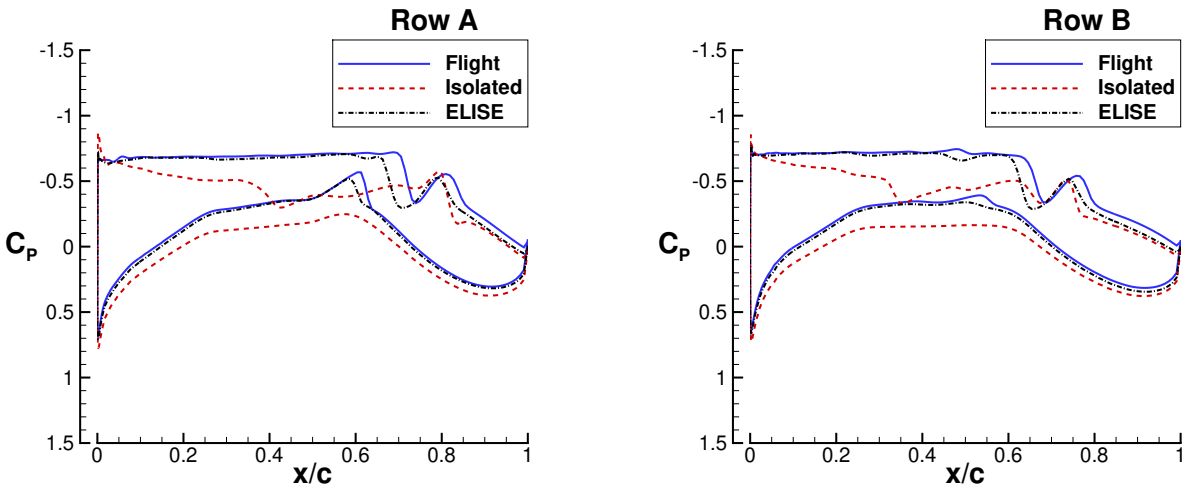

a. Row A pressure distributions.

b. Row B pressure distributions.

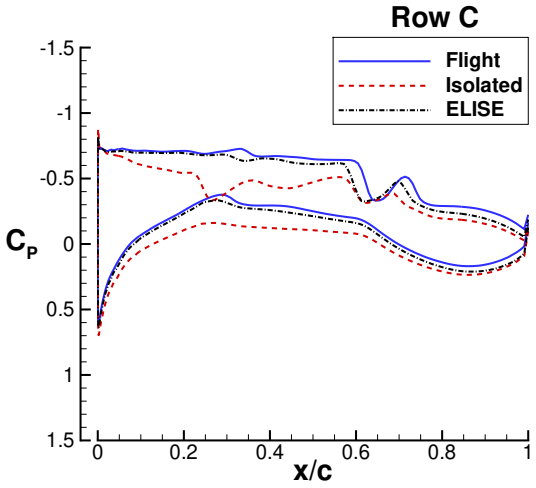

c. Row C pressure distributions.

Figure 15. Pressure distributions at the three example rows on the CATNLF test article, comparing the flow solution from the Flight Configuration grid (blue), the Isolated Configuration grid (red), and the ELISE Design (black).

An evaluation of the laminar flow characteristics of the CATNLF test article with the ELISE surface is required to assess the effectiveness of the design. One goal is that the transition location is predicted similarly with both the F-15 and the ELISE geometries. However, since the ELISE geometry would be used in computational studies to develop transition prediction capabilities, it is of equal importance that the physics behind the transition agrees well between the configurations. For this application, the physics of interest are the boundary layer instability growth. Figure 16 shows the stability analysis results for both TS and CF at the same spanwise locations as the example pressure distributions. These plots confirm that the good agreement in pressures translates to good agreement in instability growth behavior. The CF instabilities are primarily dominant at the leading edge, and the peak CF value in that region is well matched with the introduction of the ELISE surface. The previously-discussed midchord CF regrowth seen on the Isolated Configuration is no longer present on the ELISE Design solution. The TS growth was significantly improved from the Isolated Configuration and can now be seen to gradually increase from the leading edge to the desired transition location, demonstrating the characteristics of the CATNLF design method and closely following the growth rate that is seen on the Flight Configuration. The TS instabilities of the ELISE Design show occasional deviations from the Flight Configuration as it grows due to slight pressure differences, but the overall growth behavior and magnitude is well matched.

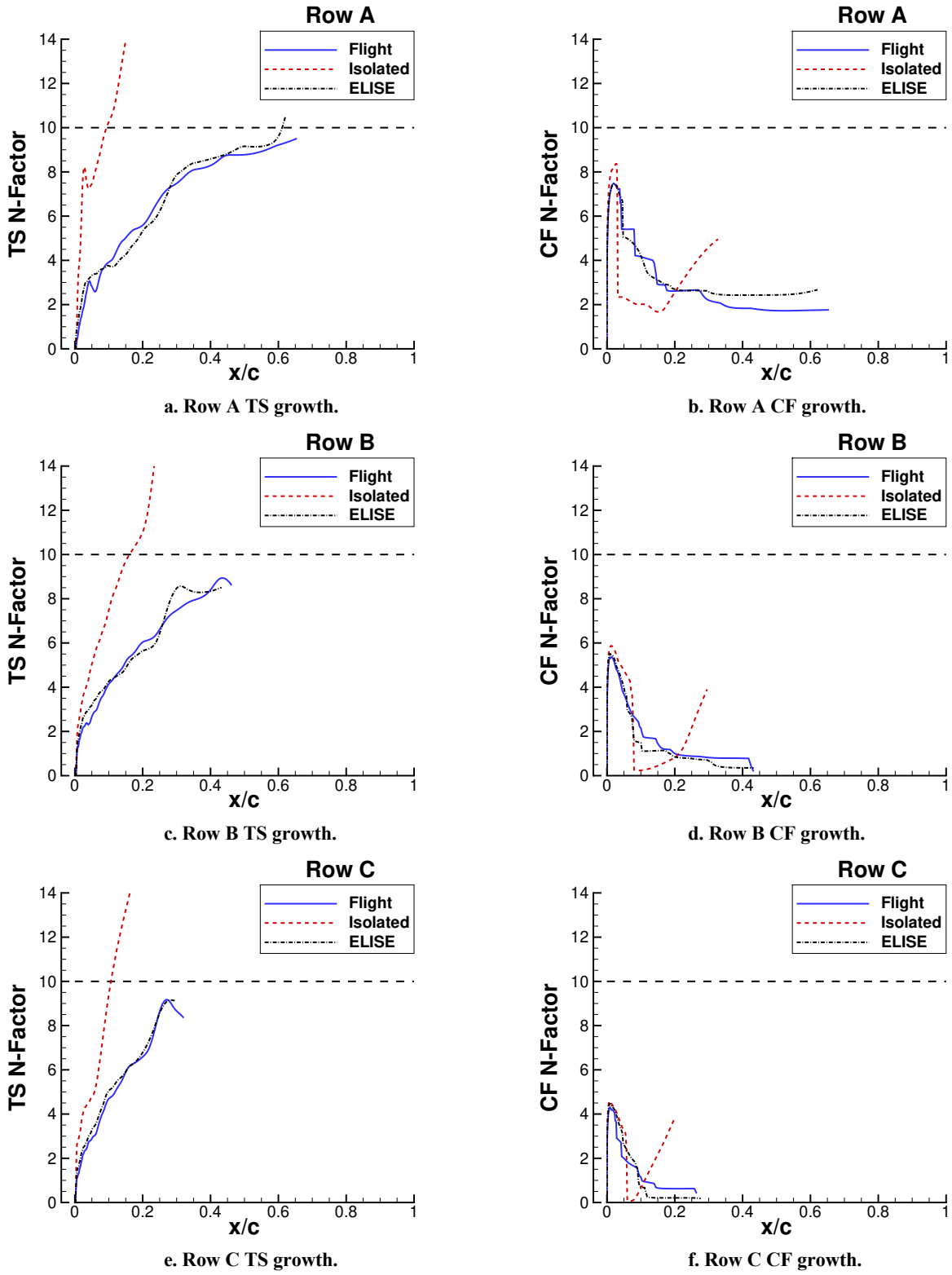

a. Row A TS growth.

b. Row A CF growth.

c. Row B TS growth.

d. Row B CF growth.

e. Row C TS growth.

f. Row C CF growth.

Figure 16. N-factor growth of both Tollmein-Schlicting (left) and crossflow (right) from the Flight Configuration grid (blue), the Isolated Configuration grid (red), and the ELISE Design (black). The horizontal dashed line at an N-factor of 10 represents the critical N-factor used in this work.

Several simple differencing techniques have been applied between the N-factor data from the Flight Configuration and the ELISE Design to help quantify differences and ensure the design reproduced the instability growth accurately enough. The first method calculates the difference in N-factor value at every point along the chord, which is labeled ΔN-factor and helps visualize any chordwise variation in N-factor agreement, as well as how closely the N-factor growth agrees along the chord. The second analysis method calculates the difference in chordwise location (i.e., x/c) for every N-factor value, labeled as Δx/c. This method performs the differencing on the first chordwise occurrence of a given N-factor, ignoring any damping and regrowth in the N-factor curves that would cause multiple occurrences of a specific N-factor value. The Δx/c value helps quantify the agreement in the transition location between the solutions if the critical N-factor was different than 10. These two differencing methods are most helpful when analyzing TS, where the goal is to match the gradual growth in TS from the leading edge to the transition location. Due to the chordwise distribution of CF growth, the primary metric for CF agreement would be matching the peak CF value near the leading edge because this feature is what would cause CF transition if it grew high enough. An example of the simple differencing methods is shown in Figure 17.

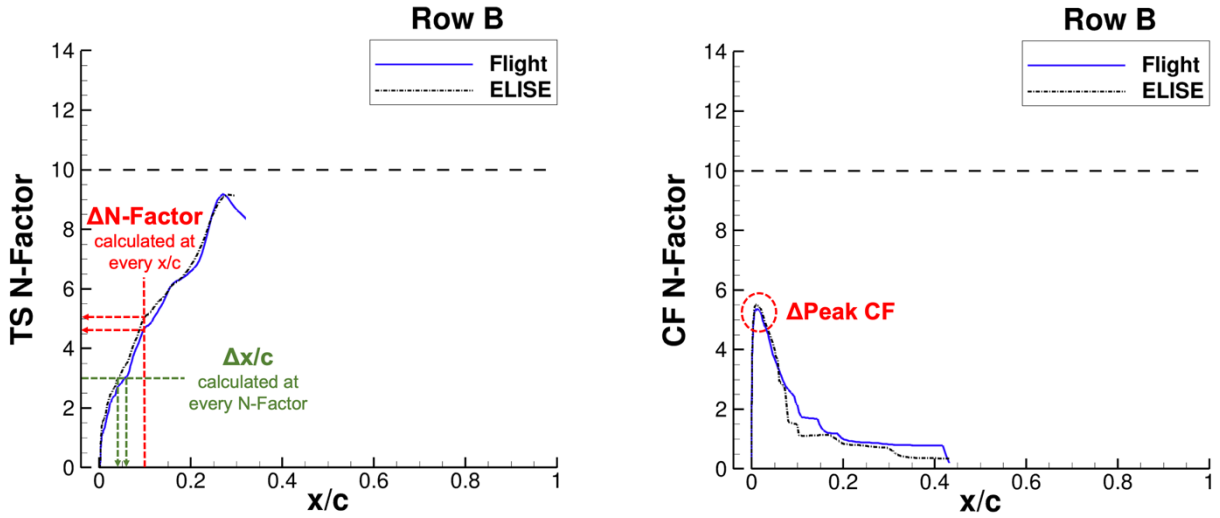

a. Example differencing on TS growth.

b. Example differencing on CF growth.

Figure 17. Example N-factor growth plot of TS (left) and CF (right) showing the differencing techniques applied to quantify differences between the Flight Configuration (blue) and the ELISE Design (black).

Figure 18 shows the spanwise variation of the two differencing techniques applied to TS to provide an example of the type of data used for these analyses. The inboard two stations and tip station were removed from the analysis because no laminar flow is expected at those locations. The average and maximum values from each spanwise location are included. The ΔN-factor spanwise data in Figure 18a illustrate that the development of TS over the chord is consistent across the span of the test article. The ΔN-factor is slightly higher inboard, but overall the average spanwise agreement is well below 1 N-factor. Given the assumptions and uncertainties involving N-factor applications, a spanwise average ΔN-factor value of 0.33 seems reasonable for most use cases of this dataset. The Δx/c spanwise data in Figure 18b lead to a similar conclusion of acceptable agreement. The average Δx/c data show a very slight increase in difference inboard compared to outboard, but overall remain low across the span. The peak CF comparison is found in Figure 19. While CF is not expected to cause transition at this flow condition, it is still valuable to find excellent agreement in peak CF values across the span. A summary of the differencing values is included in Table 3. Overall these values suggest very good agreement between both the TS and CF N-factor development for the two configurations.

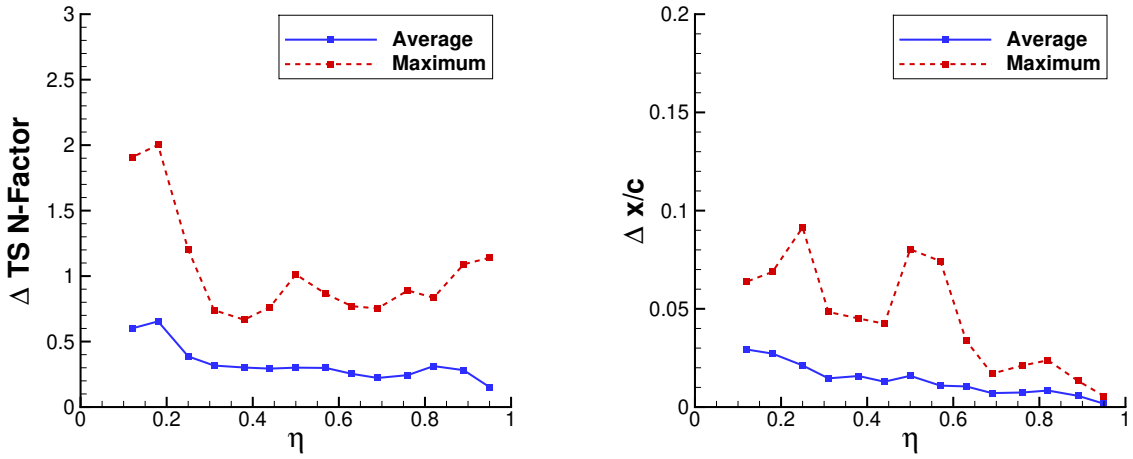

a. ΔN-factor on TS growth out the span. **b. Δx/c on TS growth out the span.**

Figure 18. Spanwise distributions of the ΔN-factor (left) and the Δx/c (right) for TS growth between the Flight Configuration and ELISE Design solutions. The average and maximum values from each station are shown.

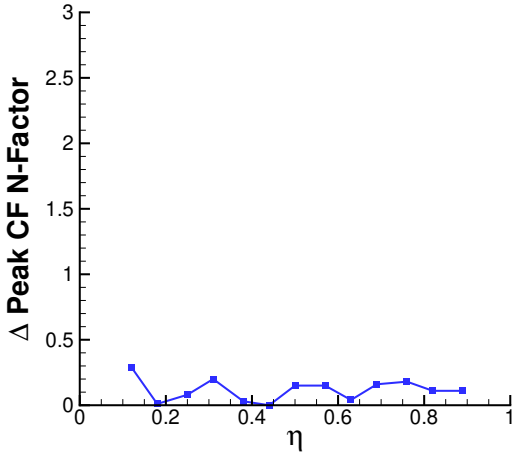

Figure 19. Spanwise distribution of the ΔPeak CF N-factor between the Flight Configuration and the ELISE Design solutions.

Table 3. Delta values between the Flight Configuration and the ELISE Design solutions.

Δ TS N-factor	Average	0.33 N-Factor
	Maximum	2.00 N-Factor
Δ x/c for TS	Average	0.01 x/c
	Maximum	0.09 x/c
Δ Peak CF	Average	0.12 N-Factor
	Maximum	0.29 N-Factor

An additional evaluation of the success of the ELISE Design can be performed based on predicted transition locations. A planform view of the CATNLF test article with the predicted transition fronts associated with a critical N-factor level of 10 can be seen in Figure 20. The image confirms that the introduction of the ELISE surface significantly altered the transition location, and that the ELISE Design transition location aligns well with the Flight Configuration across the span of the test article. The percentage of surface area expected to be laminar for the Flight Configuration, Isolated Configuration, and ELISE Design are 40.8%, 11.6%, and 42.4%, respectively. The significant

improvement in laminar flow extent from the Isolated Configuration to the ELISE Design Configuration provides confirmation of the magnitude of impact the ELISE design had on the CATNLF test article. A spanwise distribution of the magnitude of difference in transition locations is found in Figure 21. The average difference in predicted transition location is 4.2% chord, which is smaller than the anticipated accuracy capability of determining the transition location from the transition visualization images in the flight test data, estimated at around 5% chord. This level of agreement in predicted transition location, along with the pressure distributions and N-factor growth correlation, suggest that the designed ELISE surface was successful at replicating the aerodynamic influence of the F-15 vehicle on the CATNLF flight test article at the design condition.

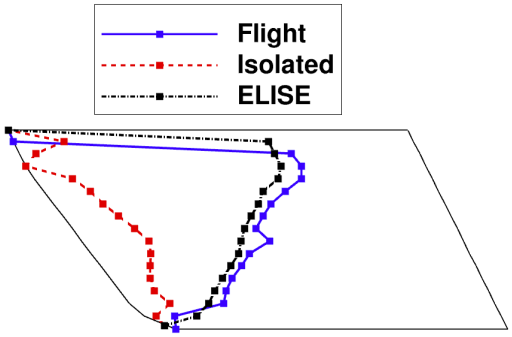

Figure 20. Planform view of the test article showing the predicted transition locations from the Flight Configuration (blue), the Isolated Configuration (red), and ELISE Design solutions.

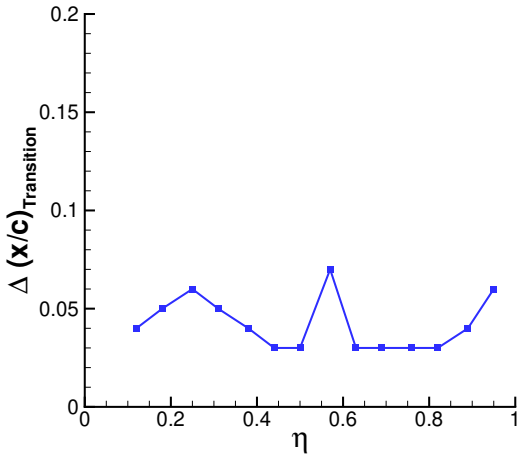

Figure 21. Spanwise distribution of the difference in chordwise transition location between the Flight Configuration and the ELISE Design solutions.

B. Off-Design Assessment

The plan for the flight test is to primarily fly at or very near the design conditions during data acquisition, namely Mach 0.85 and 0 degrees angle of attack and sideslip, while changing altitude to alter the Reynolds number on the test article. It is also desirable to obtain data at slight off-design conditions, including small perturbations in Mach and sideslip, to evaluate the sensitivity of the test article laminar flow. Additionally, there is an anticipated variation on the desired conditions based on pilot ability to hold conditions during data acquisition. It can be expected that the interference effects from the complex F-15 geometry will change at off-design conditions. As such, it is valuable to evaluate how well the ELISE surface replicates the influence of the F-15 at small off-design conditions. This subsection presents data obtained to investigate this, as well as discussions on potential limitations or use cases for the ELISE surface.

To assess the ability of the ELISE surface to replicate the aerodynamic influence of the F-15 at off-design conditions, small variations in Mach and sideslip angle were analyzed. The ranges of the parameters is based on expected ranges in the flight test data determined by pilot controllability. For the Mach off-design analysis, ±0.02 Mach were evaluated in 0.01 increments, and for sideslip angle, ±1.0 degrees were evaluated in 0.5 degree increments. A change in sideslip angle will produce an effective angle-of-attack change on the test article due to its vertical fin-like orientation relative to the freestream flow angle.

For brevity, only the transition fronts are included in this report, as any agreement in that data is a direct result of an agreement in the pressure distributions and TS and CF growth. Figure 22 shows the transition fronts for the Flight Configuration (blue) and ELISE Design (red) for the four off-design Mach numbers evaluated. The two solutions are observed to agree well throughout the range, with a slightly larger deviation between the curves at the higher Mach value of 0.87. The source of the discrepancy at the Mach 0.87 condition is likely due to the shock location difference between the two solutions, which limits the laminar flow extent. This magnitude of shock location difference was not seen at the lower Mach numbers. Similar transition front data for the sideslip conditions can be found in Figure 23. In general, the sideslip conditions appear to more negatively impact the agreement between the Flight Configuration and ELISE Design solutions compared to the Mach excursions. Positive sideslip angles (i.e., negative effective angle of attack on the test article) lead to larger discrepancies in the transition locations than the negative sideslip angles. Upon investigation of the pressures, the two solutions differ in the shock location at the more positive sideslip angles. The low sideslip angles show better agreement, with the -1.0 degree condition agreeing well over the outboard portion of the wing in spite of the larger inboard differences.

To help visualize the agreement between the transition front data, the average difference in chordwise transition location ($\Delta(x/c)_{Transition}$) at each station is presented in Figure 24. A horizontal dashed line at $\Delta(x/c)_{Transition}$ of 0.05 is included to represent a proposed acceptable agreement level, based on the uncertainty that is expected in determining the transition front from the flight test transition images. This figure shows that all Mach numbers except for the highest evaluated (Mach 0.87) fall below the recommended acceptable level of agreement. This would suggest that the ELISE surface could be used for experimental data that fall within the range of Mach 0.83 to 0.86. Similarly, the sideslip data can be used to establish a recommended range of use for a given ELISE surface. As the fronts suggested, the sideslip conditions fell outside the accepted agreement limit fairly quickly, and would result in a range of use of sideslip angles of -0.5 to 0.0 degrees. These conditions have only been evaluated for single parameters (i.e., Mach changed while sideslip held constant, and vice versa), and further investigations would be required if both parameters change at the same time to ensure the recommended ranges were consistent. For data that are beyond the recommended range of either Mach or sideslip angles, a new ELISE surface would need to be designed at a different condition to try to correct for any disagreement. This may lead to multiple ELISE surfaces, designed at different flow conditions, to cover the range of Mach or sideslip angles seen in the experimental data.

In addition to comparing the chordwise transition location, the simple differencing techniques described previously were performed on all the solutions from the Mach and sideslip conditions. The data provide a metric of agreement for the growth of the TS curves themselves, rather than just the final transition location associated with the critical N-factor level of 10, which is assumed in this work. The assessment found that the $\Delta x/c$ for TS is below 0.03 for all conditions, which suggests that, even when the shock location was predicted incorrectly and led to larger differences in transition location, the overall TS growth was remarkably similar for all the conditions. Additionally, the ΔN-factor for TS was between 0.33 and 0.69 N-factor for all eight off-design conditions, further confirming consistent TS growth between solutions. In general, the additional differencing techniques suggest that the instability growth agrees well across the full range of Mach and sideslip analyzed even when the transition locations deviate beyond the recommended value.

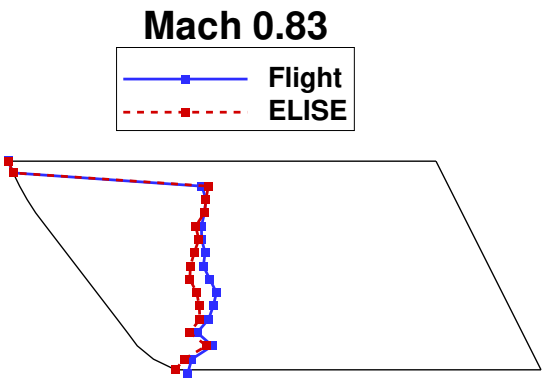

a. Transition fronts for Mach 0.83.

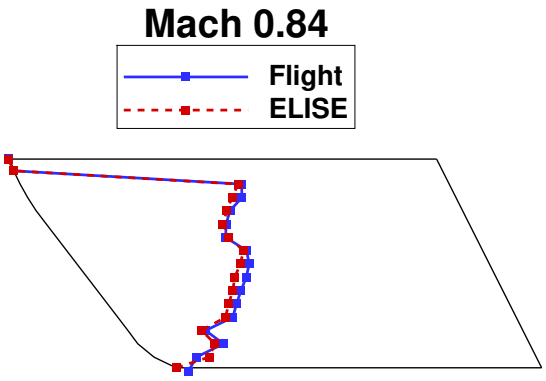

b. Transition fronts for Mach 0.84.

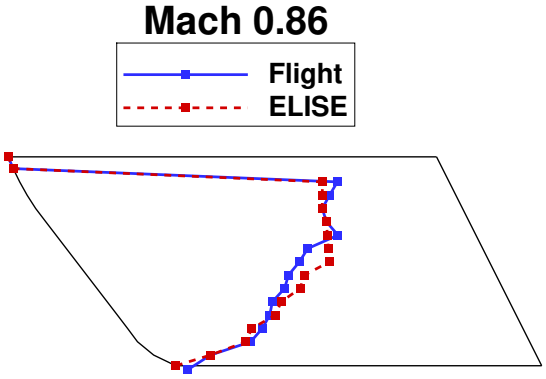

c. Transition fronts for Mach 0.86.

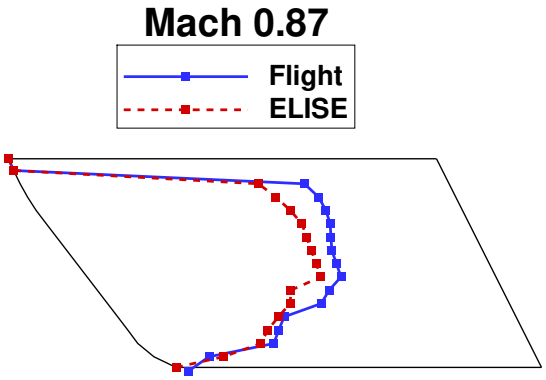

d. Transition fronts for Mach 0.87.

Figure 22. Planform view of the test article showing the predicted transition locations from the Flight Configuration (blue) and the ELISE Design (red) solutions for the off-design Mach numbers analyzed.

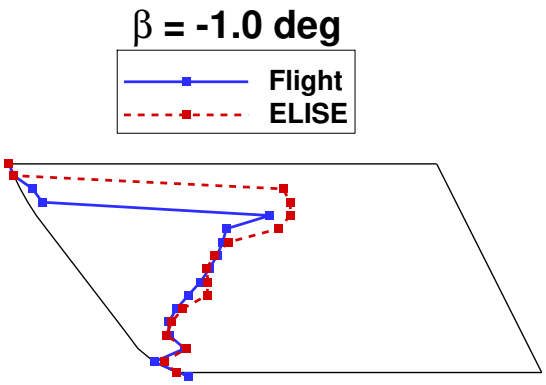

a. Transition fronts for β = -1 deg.

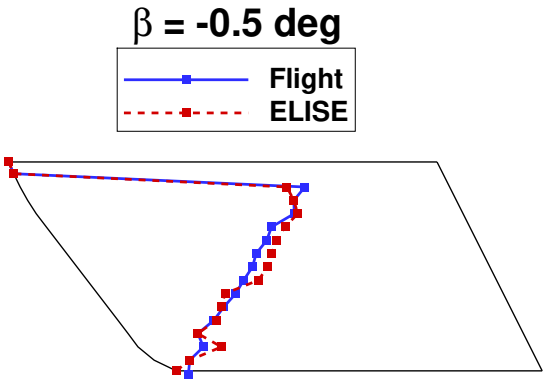

b. Transition fronts for β = -0.5 deg.

Figure 23. Planform view of the test article showing the predicted transition locations from the Flight Configuration (blue) and the ELISE Design (red) solutions for the off-design sideslip angles (β) analyzed.

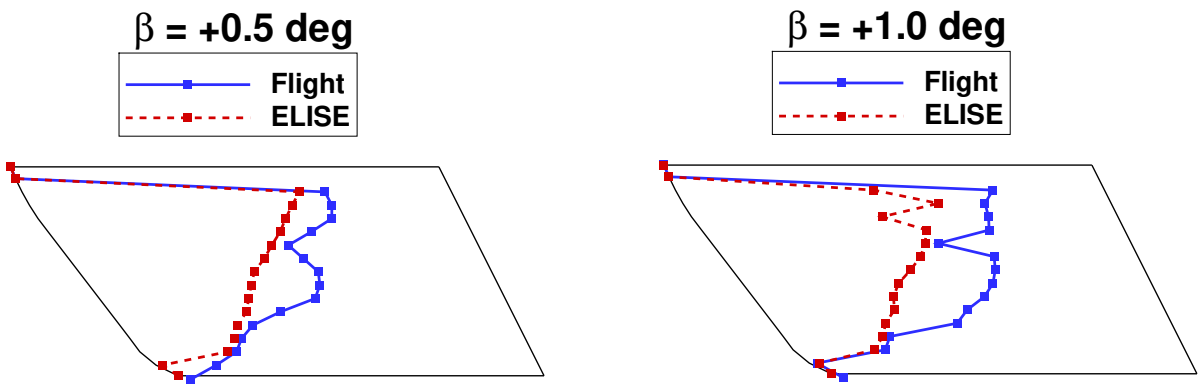

c. Transition fronts for β = 0.5 deg.

d. Transition fronts for β = 1 deg.

Figure 23 (Continued). Planform view of the test article showing the predicted transition locations from the Flight Configuration (blue) and the ELISE Design (red) solutions for the off-design sideslip angles (β) analyzed.

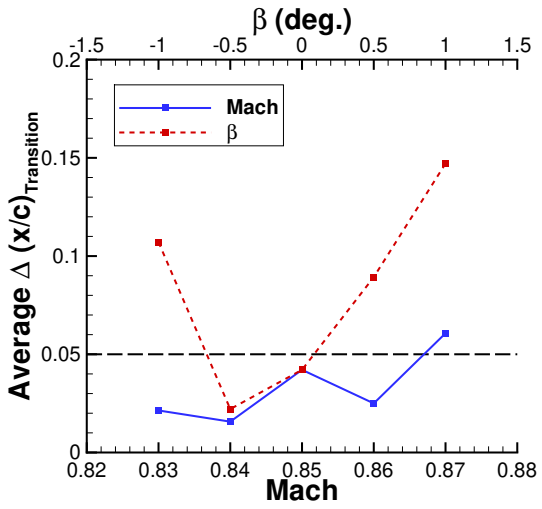

Figure 24. Average difference in chordwise transition location for off-design conditions of Mach (blue) and sideslip angle (red). The horizontal black dashed line at an Average $\Delta(x/c)_{Transition}$ of 0.05 represents a recommended acceptable difference maximum based on expected uncertainty levels in the experimental transition images.

One present limitation in the ELISE surface is related to changes in angle of attack. The ELISE surface was set up as a single-side flat plate, where the surface is directly connected to the outer boundary patch similar to how a semispan simulation would be set up. Due to the fin-like orientation of the configuration, changes in angle of attack in the flow solver results in flow going into or out of the ELISE surface and outer boundary patch. It was observed that very little change occurred on the Isolated Configuration compared to the Full Configuration when angle of attack was changed in the flow solver input, which implied that the outer boundary patch was dominating the incoming flow behavior and straightening out any angle-of-attack changes ahead of the test article. Several boundary conditions were analyzed in an attempt to find one that would not damp out the incoming flow angle of attack with limited success. The present assumption is that, due to the design surface setup, aerodynamic influence due to angle-of-attack variations cannot be modeled with the ELISE surface. Any changes in angle of attack of the flight testbed would require a redesign of the ELISE surface to properly model the influence. There will likely be small perturbations in angle of attack during data acquisition due to pilot control tolerances, and the current plan is to analyze the flight data to evaluate sensitivity to angle of attack and determine if multiple ELISE designs are needed to cover the range of flow conditions seen in the flight test. A similar analysis will be needed for Mach and sideslip angle changes if they fall outside the range of

acceptable agreement, as discussed previously. While it is not ideal to have multiple ELISE surfaces that cover only a specified range of flow conditions, the approach of providing a new geometry or grid for different flow conditions is similar to that of computational studies involving internal flow, such as a model inside a wind tunnel. Changes in the flow conditions of a model in a wind tunnel require changing the orientation of the model itself in the grid instead of a simple flow solver input change to better represent wind tunnel testing. After the flight test data are in hand, the ELISE surface will be redesigned to match the data, and an additional evaluation of off-design conditions will be performed.

IV. Additional Considerations for Wind Tunnel Applications

One area of research that is currently of interest is the impact of environment on laminar flow extents, and how to best model those impacts. There are very few experiments publicly available that have isolated the impact of environment by testing the same model in both flight and a wind tunnel. One such experiment was recently conducted by Owens et al. on a supersonic laminar flow test article, referred to as Swept Wing Laminar Flow (SWLF) [17]. The SWLF test article was flown under the F-15 using the CLIP testbed and also tested in the NASA Langley Research Center 20-Inch Supersonic Wind Tunnel (SWT). The results from this experimental campaign provide valuable insight into the impact of environment to laminar flow extent, and there is a desire to expand that research for the transonic flow regime. Initial planning has begun to provide a similar dataset for the CATNLF test article by testing it in a wind tunnel after flight testing. The SWLF model was small, non-lifting, and at different flow conditions, which led to reasonable agreement between the flight configuration and the wind tunnel setup where the F-15 and CLIP were not included. As shown in this paper thus far, that is not the case for the CATNLF test article, which experiences significant aerodynamic influence from the F-15. In order to isolate the impact of environment, the wind tunnel test would need to include a way to model the F-15 in the tunnel. Due to sizing constraints of most tunnels of interest for this work, an F-15 would not be a feasible option, necessitating something like the ELISE surface in the tunnel. Work on the design of an ELISE surface for a wind tunnel application has not yet begun, but discussions of what changes would be needed compared to the previously presented ELISE surface design are presented here.

The primary objective of the ELISE surface design in this paper was to illustrate the type of agreement possible, specifically for use in computational studies. As such, the simplest computational model was used for the design surface, namely an inviscid wall, without being constrained to realistic physics that would be present on a physical model. One clear difference for a wind tunnel application would be the necessity of modeling viscous effects on the ELISE surface. At transonic conditions, viscous effects are expected to influence the final geometry of the surface. While viscous effects would likely change the final geometry of the surface, this change to the design setup is not expected to significantly alter the conclusions shown in this paper. It is expected that a new viscous ELISE surface can be designed to provide similar success in replicating the aerodynamic influence of the F-15.

A second increase in complexity would come from the need to model the wind tunnel walls. Tunnel walls are known to alter the aerodynamics of a model, and facilities often put significant effort into minimizing these effects, such as adding relief features to the walls (slots, porosity, shapable walls, etc.), placing sizing limits on the models, and/or adding wall corrections to wind tunnel data. For an ELISE surface to be designed to mimic flight in a wind tunnel, it would be necessary to include any expected influence in the tunnel like the walls. Future work is planned to model the four walls of the test section of a proposed wind tunnel, likely either the NASA Ames Research Center 11- by 11-Foot Transonic Wind Tunnel or the NASA Langley Research Center National Transonic Facility. Both of these tunnels utilize slots to alleviate wall effects, which can be modeled in the flow solver with the porosity boundary condition. Viscous effects would be included on the walls with the aim to model the appropriate boundary layer thickness at the test section where the model is located. The ELISE surface would be treated as a tunnel liner, and is assumed to be solid with no porosity. The effect of the wind tunnel walls on the design of the ELISE surface is anticipated to be significant. There is often an increase in Mach, and potentially a change in flow angularity, associated with adding walls. The increase in Mach from wall effects may help match the F-15 better, as it was observed in the design presented in this paper that the F-15 creates an increase in Mach for the test article. However, until the design work begins, it is unknown if the wall effects will be too significant for CDISC to create a geometry that reasonably matches the target pressures.

One final change to the design for a wind tunnel application would be sizing limitations. While the initial ELISE surface was sized to fit in two potential tunnels, there are no practical limitations on the size or shape of an ELISE surface for use in computational studies. However, in a tunnel environment, blockage concerns impose size limitations on what can be tested in a facility at a given flow condition. Sizing constraints would need to be included during the design process. As briefly mentioned previously, the current design effort did explore design space limitations to try to minimize the final size of the surface. It was found that only a small spanwise (left/right width direction) region

was needed, and that limiting the chordwise (length direction) design region reduced the final height of the bumps. The wind tunnel application design would leverage these lessons learned, but would likely need further refinement to meet the strict sizing constraints. Similar to the wall effects, it is unknown at this time if an ELISE surface can be designed that meet the blockage criteria in a wind tunnel facility.

Several changes would be needed to the design setup for a wind tunnel application that will likely make the design significantly more challenging. Future work is planned to pursue an ELISE surface compatible with a wind tunnel. Any plans for testing the CATNLF flight test article is subject to the conclusions of flight test data and project priorities.

V. Concluding Remarks

The CATNLF flight test campaign is comprised of three experiments that utilize the existing CLIP testbed at Armstrong Flight Research Center underneath an F-15. The primary experiment is the CATNLF test article, which is a short-span wing-like model designed with the CATNLF method to enable large extents of laminar flow at transonic transport conditions. The test article is instrumented and the flight conditions are selected in such a way that the flight test is expected to provide a robust set of laminar flow experimental data. While the primary objective of the test is for the researchers to learn more about the CATNLF method, there is a desire to open the dataset to others to aid in computational transition prediction advancements. In order for the computational community to utilize the dataset, the geometry of the test setup would need to be included so that it can be modeled computationally. However, the F-15 is not a releasable geometry, and cannot be provided publicly. As this paper shows, simply removing the F-15 significantly alters the flow field around the CATNLF test article and leads to dramatically altered laminar flow characteristics. Using the isolated CATNLF test article with the experimental flight test data would lead to mismatched flow conditions and faulty conclusions or calibrations.

Knowing the limitations with releasing the F-15 geometry and the impact the vehicle has on the CATNLF test article, a research effort was initiated to design a surface that reproduces the same aerodynamic interference as the F-15 on the test article. A remote design approach was developed within the CDISC aerodynamic design tool to accomplish this objective, which is referred to as ELISE. Target pressures used for CDISC design were created from modified F-15 surface pressures and the ELISE surface was altered to produce the desired surface pressures. The final design created two asymmetrical bumps, one on either side of the test article, which reproduced the flow field seen underneath the F-15. The success of the ELISE design was evaluated on the agreement of surface pressures and laminar flow characteristics (i.e., TS and CF growth). The average difference between the flight configuration with the F-15 and the ELISE design configuration in chordwise transition location on the test article was 4.2% chord at the design condition. This level of agreement is expected to be less than the uncertainty of the experimental transition location in the flight test and was therefore considered a successful ELISE design. In addition to the primary design condition, several off-design conditions were analyzed to evaluate if the ELISE design adequately produced the F-15 interference effects at other expected flight conditions. In general, the agreement in pressures and laminar flow characteristics were maintained reasonably well at the Mach and sideslip angles evaluated, with sideslip causing larger differences, resulting in a more limited suggested range of use for the current ELISE design. An angle-of-attack change is not be possible with the ELISE design due to the way the surface is modeled in the flow solver.

Discussions were presented regarding future work related to the ELISE design method to create a wind tunnel liner for a proposed wind tunnel test of the CATNLF test article. Additional future work is needed once the flight test data are in hand to fine-tune the ELISE design geometry to ensure the match to the flight test data is still adequate. There are also plans to evaluate the ELISE design geometry in additional flow solvers to ensure the CATNLF test article pressures and characteristics are reasonably matched across multiple codes. The remote design approach developed in this work provides a reasonable path forward to allow public use of the CATNLF flight test data, and may have additional applications for other projects in which producing specific aerodynamic interference effects are needed.

Acknowledgments

This work was sponsored by the NASA Advanced Air Transport Technology (AATT) Project, which is part of the Advanced Air Vehicles (AAVP) in the NASA Aeronautics Research Mission Directorate (ARMD). Resources supporting some computational results in this paper were provided by the NASA High-End Computing (HEC) Program through the NASA Advanced Supercomputing (NAS) Division. The CATNLF Flight Test team is comprised of researchers, engineers, and technicians across the NASA Langley Research Center and the NASA Armstrong Flight Research Center.

References

[1] Lynde, M.N., Campbell, R.L., Hiller, B.R., and Owens, L.R., "Design of a Crossflow Attenuated Natural Laminar Flow Flight Test Article," AIAA 2021-0173, January 2021.

[2] Campbell, R.L. and Lynde, M.N., "Natural Laminar Flow Design for Wings with Moderate Sweep," AIAA 2016-4326, June 2016.

[3] Lynde, M.N. and Campbell, R.L., "Expanding the Natural Laminar Flow Boundary for Supersonic Transports," AIAA 2016-4327, June 2016.

[4] Lynde, M.N. and Campbell, R.L., "Computational Design and Analysis of a Transonic Natural Laminar Flow Wing for a Wind Tunnel Model," AIAA 2017-3058, June 2017.

[5] Lynde, M.N., Campbell, R.L., and Viken, S.A., "Additional Findings from the Common Research Model Natural Laminar Flow Wind Tunnel Test (Invited)," AIAA-2019-3292, June 2019.

[6] Lynde, M.N., Campbell, R.L., Rivers, M.B., Viken, S.A., Chan, D.T., Watkins, A.N., and Goodliff, S.L., "Preliminary Results from an Experimental Assessment of a Natural Laminar Flow Design Method," AIAA 2019-2298, January 2019.

[7] Rivers, M.B., Lynde, M.N, Campbell, R.L., Viken, S.A., Chan, D.T., Watkins, A.N., and Goodliff, S.L., "Correction: Experimental Investigation of the NASA Common Research Model with a Natural Laminar Flow Wing in the NASA Langley National Transonic Facility," AIAA 2019-2189, January 2019.

[8] Choudhari, M.M., "Transition Modeling and CFD Vision 2030, AIAA Transition Modeling Workshop-I," Website Accessed November 2023, [https://transitionmodeling.larc.nasa.gov/workshop_i/].

[9] Frederick, M.A. and Banks, D.W., "Flight Tests of a Supersonic Natural Laminar Flow Airfoil," NASA/TM 2015-218940, December 2015.

[10] Watkins, A.N., Peak, S.M., Goodman, K.Z., Frederick, M.A., and Hulgan, J.T., "Flight Test of a Resistive Heating Coating for Visualizing Flow Transition," AIAA 2020-3089, June 2020.

[11] Pandya, M.J., Jespersen, D.C., Diskin B., Thomas, J.L., and Frink, N.T., "Efficiency of Mixed-Element USM3D for Benchmark Three-Dimensional Flows," AIAA Journal (2021), 59(8), pp. 2997-3011; DOI: 10.2514/1.J059720.

[12] Pandya M.J., Jespersen, D.C., Diskin B., Thomas, J.L., and Frink, N.T., "Verification and Scalability of Mixed-Element USM3D for Benchmark Three-Dimensional Flows," AIAA Journal (2021), 59(11), pp. 4719-4738; DOI: 10.2514/1.J060064.

[13] Campbell, R.L., "Efficient Viscous Design of Realistic Aircraft Configurations," AIAA-98-2539, June 1998.

[14] Campbell, R.L., Banchy, M.N., and Hiller, B.R., "History and Status of the CDISC Aerodynamic Design Method," AIAA SciTech Forum 2024, January 2024.

[15] Wie, Y.S., "BLSTA: A Boundary Layer Code for Stability Analysis," NASA CR 4481, 1992.

[16] Chang, C.L., "The Langley Stability and Transition Analysis Code (LASTRAC): LST, Linear and Nonlinear PSE for 2-D, Axisymmetric, and Infinite Swept Wing Boundary Layers," AIAA 2003-0974, 2003.

[17] Owens, L.R., Beeler, G.B., King, R.A., Chou, A., Balakumar, P., and Banks, D.W., "Supersonic Traveling Crossflow Wave Characteristics in Ground and Flight Tests," AIAA 2020-0777, January 2020.